nature chemistry

ARTICLES

https://doi.org/10.1038/s41557-019-0376-9

Capturing intrinsic site-dependent spectral signatures and lifetimes of isolated OH oscillators in extended water networks

Nan Yang[1], Chinh H. Duong[1], Patrick J. Kelleher[1,2] and Mark A. Johnson[1]*

The extremely broad infrared spectrum of water in the OH stretching region is a manifestation of how profoundly a water molecule is distorted when embedded in its extended hydrogen-bonding network. Many effects contribute to this breadth in solution at room temperature, which raises the question as to what the spectrum of a single OH oscillator would be in the absence of thermal fluctuations and coupling to nearby OH groups. We report the intrinsic spectral responses of isolated OH oscillators embedded in two cold (~20 K), hydrogen-bonded water cages adopted by the $Cs^+\cdot(HDO)(D_2O)_{19}$ and $D_3O^+\cdot(HDO)(D_2O)_{19}$ clusters. Most OH oscillators yield single, isolated features that occur with linewidths that increase approximately linearly with their redshifts. Oscillators near 3,400 cm^{-1}, however, occur with a second feature, which indicates that OH stretch excitation of these molecules drives low-frequency, phonon-type motions of the cage. The excited state lifetimes inferred from the broadening are considered in the context of fluctuations in the local electric fields that are available even at low temperature.

The microscopic mechanics that underlie the diffuse OH stretching spectrum of condensed phase water in all its forms (liquid, solid and interface) is currently under intense study as theoretical[1–8] and experimental[9–16] advances are becoming capable of handling the cooperative interactions that drive its macroscopic behaviour. Most of the breadth displayed by the OH stretching region persists even when OH oscillators are decoupled through isotopic dilution to isolate the response of HDO when surrounded by a thermally fluctuating D_2O matrix[17]. Most often, simulations of the infrared spectrum adopt the ansatz that, if the surrounding local structure could be frozen in place, an isolated OH oscillator would contribute a single feature with an intrinsic width associated with the vibrational lifetime[18], determined by the topology of the surrounding hydrogen-bonding network[19]. In this case, the breadth of the OH stretching manifold can be recovered by averaging over the many different structures present in the thermal ensemble[20]. The situation in the liquid is, of course, dynamic in the sense that a single OH oscillator explores all available configurations on the very fast timescale associated with spectral diffusion[21,22]. Here we present experimental results that test two fundamental questions regarding this ansatz. The first involves the degree to which the vibrational signature of a local oscillator is actually confined to the vibrational fundamental, and the second pertains to the dependence of the intrinsic lineshapes on their locations within the OH stretching envelope. The first issue arises because several recent studies reported strong combination bands that correspond to the excitation of soft modes along with the OH fundamentals in small cluster systems at a very low temperature[23–25], which raises the question of whether such mechanics are also at play in larger networks. The second issue regards the lifetimes of the OH($v=1$) excited states at 0 K and how these depend on their locations in the spectrum. Related aspects of these questions can be probed with two-dimensional infrared spectroscopy, and it is established that the lifetimes of the OH($v=1$) vibrational levels (population relaxation) are on the order of picoseconds, which sets a lower limit on the homogeneous linewidths of about 10 cm^{-1} (refs [15,26,27]). The timescales for spectral diffusion, however, are significantly shorter, with frequency modulations due to fluctuations in the O–O distances estimated to be about an order of magnitude faster[6,15,28,29]. These ultrafast processes in liquid water at high temperature obscure contributions to the broadening that are intrinsic to the local environment, that is, those that would occur even if the local surroundings were static. The goal of this study is to reveal these heretofore hidden dynamics.

Results and discussion

In this report, we demonstrate how the spectral signature of a single OH group embedded in an extended, quasi-rigid hydrogen-bond network can be experimentally determined by exploiting the unique properties of cold, size-selected cluster ions. The minimum requirements for a useful model system that can accomplish this are that it has to display sufficient variation in the local binding motifs so that its OH stretching fundamentals span the range observed for bulk water, and have a high enough density of states in the 3,000–4,000 cm^{-1} region to provide an effective continuum of background quantum states that can interact with the excited OH group. These criteria are met by the 'magic' cluster ions with the structures indicated in Fig. 1: $Cs^+\cdot(H_2O)_{20}$, which encapsulates the central Cs^+ ion in a distorted pentagonal dodecahedron (PD) cage, and $H_3O^+\cdot(H_2O)_{20}$, which offers a radically different PD arrangement in which the hydronium ion resides on the surface of the cage[30,31]. Specifically, we isolated the $Cs^+\cdot(HDO)(D_2O)_{19}$ and $D_3O^+\cdot(HDO)(D_2O)_{20}$ isotopologues at low temperature using cryogenic mass spectrometry methods and measured the spectral signatures of a single OH group that resided in each of their many topologically distinct sites. This is accomplished with the use of isotopomer-selective, two-colour infrared–infrared photofragmentation spectroscopy[23]. An important aspect of the PD structures is that most (in some cases all) of the network sites are distinguishable in the many distinct, nearly isoenergetic hydrogen-bonding arrangements. (Note that the PD_0 structure in Fig. 1a is the specific isomer from Schulz and Hartke[30].)

[1]Sterling Chemistry Laboratory, Yale University, New Haven, CT, USA. [2]Present address: Department of Chemistry, University of Virginia, Charlottesville, VA, USA. *e-mail: mark.johnson@yale.edu

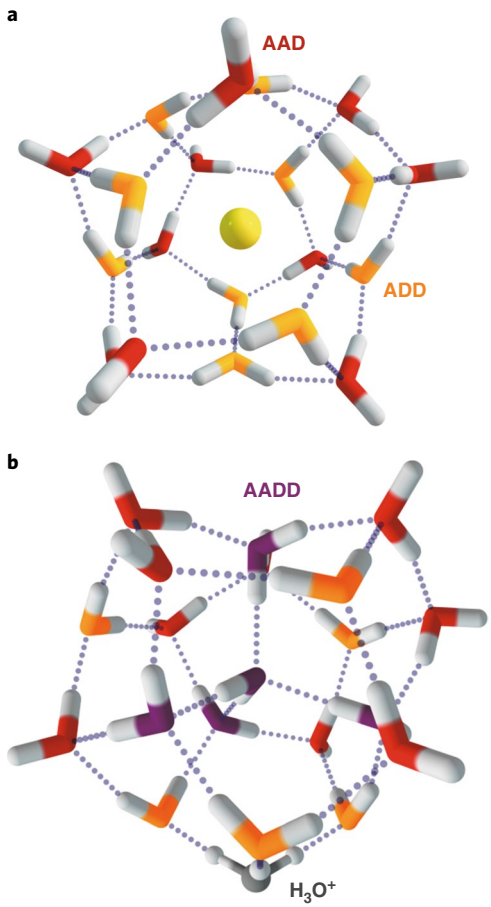

Fig. 1 | Representative structures of the pentagonal dodecahedron (PD_0) water cages. a,**b**, The representative $Cs^+\cdot(H_2O)_{20}$ cluster structure[30] (**a**) and the minimal energy structure[31] (**b**) of $H_3O^+\cdot(H_2O)_{20}$. These structures contain three classes of network sites: AAD (red), ADD (orange) and AADD (purple), which differ by the number of hydrogen-bond acceptors (A) and donors (D) associated with each water molecule. Rotatable PDF versions of the structures are given in Supplementary Fig. 1.

This diversity of local environments is a useful feature when using these clusters to explore the molecular behaviour of interfacial water because it enables spectroscopic characterization of their intrinsic behaviour in a static ensemble. That is, the cage is structurally more similar to the liquid water surface than it is to the regular order presented by crystalline ice[32,33]. This property was recently exploited to understand the spectral signature of a single H_2O molecule trapped in each site using isotopomer-selective spectroscopy on the cryogenically cooled $Cs^+\cdot(H_2O)(D_2O)_{19}$ clusters[34]. That study revealed the site dependence of the correlated absorptions between the two OH groups on the same water molecule. Here we are concerned with the spectroscopic signature associated with a single OH group located in each of the various sites in the PD structures, information that was obscured in the previous study due to complexities that arose from the intramolecular coupling between the two OH groups and with the overtone of the intramolecular HOH bend.

The vibrational spectra of the cold cluster ions were obtained using the mass messenger or 'tagging' technique[35], which yields the spectrum of mass selected ions in an action mode by resonant infrared-induced photoevaporation of the weakly bound D_2 molecules[36,37]. Figure 2b presents the $Cs^+\cdot(HDO)(D_2O)_{19}$ spectrum in the OH stretching region, along with that of $Cs^+\cdot(H_2O)_{20}$ in Fig. 2a (reproduced from Yang et al.[34]). Note that the partially resolved transitions span the range from the sharp free OH transition near 3,700 cm^{-1} to about 3,000 cm^{-1}, with bands dispersed throughout. This behaviour indicates that the single OH group can be trapped in most if not all the spectroscopically distinct hydrogen-bonding sites available in the PD structure, a situation discussed at length in Yang et al.[34] for the case of a single H_2O molecule in the otherwise perdeuterated PD cage. The nature of the hydrogen-bonding sites in play at various locations in the spectrum was established in the previous study of the $Cs^+\cdot(H_2O)(D_2O)_{19}$ isotopomers[34], and differs according to the number of donor (D) and acceptor (A) hydrogen-bonding interactions at play in each network site. Using the double resonance approach described below[34], we determined the locations in the spectrum that arise from the two OH groups on the same water molecule as a function of the site occupied by that molecule. The AAD sites contribute the free OH bands (OH^{free}_{AAD}, red in Fig. 2a,b) as well as all the spectral features below 3,450 cm^{-1}. The latter are associated with excitation of the companion OH group bound in the cage (OH^{b}_{AAD}, purple in Fig. 2a,b and Supplementary Fig. 2). The ADD sites exclusively account for the moderately redshifted features around 3,500 cm^{-1} (yellow in Fig. 2b and Supplementary Fig. 2). Note that the prominent feature (turquoise in Fig. 2a) at 3,200 cm^{-1} in the $Cs^+\cdot(H_2O)_{20}$ spectrum is missing in that of $Cs^+\cdot(HDO)(D_2O)_{19}$, which confirms its assignment to a Fermi-resonance-activated HOH bend overtone. The suppression of this feature occurs because the bend overtone of HOD occurs at ~2,800 cm^{-1}, well below the range of the OH stretching manifold. A detailed comparison of the shapes is presented in Supplementary Fig. 3.

The key to this study is that, when the clusters are sufficiently cold to suppress migration of the isotopic label among the available sites, the ensemble of clusters is heterogeneous such that the spectral signatures arising from OH occupation in each site can be isolated. This is accomplished by carrying out two-colour, infrared–infrared photobleaching measurements on the $Cs^+\cdot(HDO)(D_2O)_{19}$ and $D_3O^+\cdot(HDO)(D_2O)_{19}$ isotopologues. In this approach, a probe laser is tuned to a particular transition in the spectrum, and the population of ions responsible for that feature is monitored continuously while another, powerful pump laser is scanned through the entire spectrum upstream from the interaction with the probe laser. When the pump laser excites any transition shared by the species which is monitored by the probe frequency, the reduction in ion population yields a series of dips in the probe signal, and thus reveals all the transitions and line broadening (beyond the ~5 cm^{-1} bandwidth of the infrared lasers) associated with OH occupation in a particular site[38,39].

The traces in Fig. 2c present the isotopomer-selective dip spectra obtained by fixing the probe laser at the 16 different energies indicated by the arrows above the dip features in each trace. We emphasize that this behaviour probably does not reflect that of a single structure, but rather of an ensemble that consists of many PD isomers that are structurally similar and close in energy[30]. Note that most of the dips appear as single features centred about the probe laser energy, which thus establishes that the spectrum of the $Cs^+\cdot(HDO)(D_2O)_{19}$ isotopologue (Fig. 2b) is, indeed, heterogeneous at 20 K. It is significant, however, that the transition probed at 3,415 cm^{-1} (trace c12 in Fig. 2c and Supplementary Fig. 4) yields a pronounced second feature (indicated by a bracket), displaced from the fundamental by 51 cm^{-1}.

To gauge whether the doublet structure in the spectrum of the $Cs^+\cdot(HDO)(D_2O)_{19}$ isotopomer with an OH fundamental at 3,415 cm^{-1} is representative of more general behaviour, we extended the study to include several photobleaching measurements on the $D_3O^+\cdot(HDO)(D_2O)_{19}$ cluster. That system was chosen because it introduces additional variation in the topology of the PD network sites, which includes four-coordinated AADD molecules that are calculated to yield the largest redshifts[40]. Whereas the bands at

the extremes of the OH stretching manifold in the D_3O^+·(HDO)$(D_2O)_{19}$ spectrum (Fig. 3, traces b1 and b4) yield single OH stretching features in the photobleaching scans, probing the peak near the centre of the envelope at ~3,400 cm^{-1} generates two peaks (Fig. 3, trace b3) that are very well defined with a separation of 60 cm^{-1}. Note that this value is very close to that (51 cm^{-1}) observed in the Cs^+·(HDO)$(D_2O)_{19}$ case, as illustrated by the comparison displayed in Supplementary Fig. 4b,c. The appearance of multiple bands in photobleaching spectra can signal the interconversion between isotopomers (that is, spontaneous migration of the OH group between sites)[38]. In the present case, however, the fact that the two strong dips only appear when probing the higher energy feature (traces b2 and b3 in Fig. 3) indicates that the upper band is due to the excitation of a second transition that arose from the same ground state responsible for the OH stretching fundamental, but displaced by 60 cm^{-1} above it. The relative intensities of the two features can be recovered in a simple model that includes the relative cross-sections of the fundamental and a second, weaker band in the limit of partial optical saturation, as discussed in detail in Supplementary Section III. This is characteristic behaviour of OH groups that are anharmonically coupled to soft skeletal modes of the surrounding medium[41]. In this case, the second feature is due to an infrared-active combination band that involves the excitation of a soft (~60 cm^{-1}) mode along with the $v=1$ level of the OH stretch. The animated displacements of several representative normal modes in this energy range are given in the Supplementary Information. It is interesting that, in the case of the water cages, this soft-mode activity occurs for oscillators near 3,400 cm^{-1}, the spectral region that was recently revealed (in the Cs^+ cage) to be the cross-over point for H_2O molecules that reside in the AAD and ADD binding motifs (ADD above ~3,400 cm^{-1} and AAD below)[34]. It therefore appears that OH oscillators close to this boundary are particularly strongly coupled to soft modes of the cages in both H_3O^+ and Cs^+ systems. The appearance of such anharmonic features on the excitation of OH groups with frequencies near the centre of the diffuse OH stretching band is significant because this additional complexity has not been anticipated in spectral simulations of either the cluster systems or interfacial water[19].

On closer inspection of the dip patterns in Figs. 2 and 3, it is evident that there is a systematic increase in the widths of the dips as the probe laser is tuned to increasingly redshifted transitions in both systems. These band profiles were fit to Gaussian lineshapes (Supplementary Figs. 5 and 6), with the dependence of the full-width at half-maximum (FWHM) on the redshift ($\Delta\nu_{red}$, relative to the gas phase free OH fundamental at 3,706 cm^{-1}) presented in Fig. 4 for Cs^+·(HDO)$(D_2O)_{19}$ and D_3O^+·(HDO)$(D_2O)_{19}$. We note that not all the envelopes are Gaussian and, indeed, the dip profile of the 3,250 cm^{-1} feature in the Cs^+·(HDO)$(D_2O)_{19}$ spectrum is asymmetrical, with an embedded sharper feature (trace c15). Nonetheless,

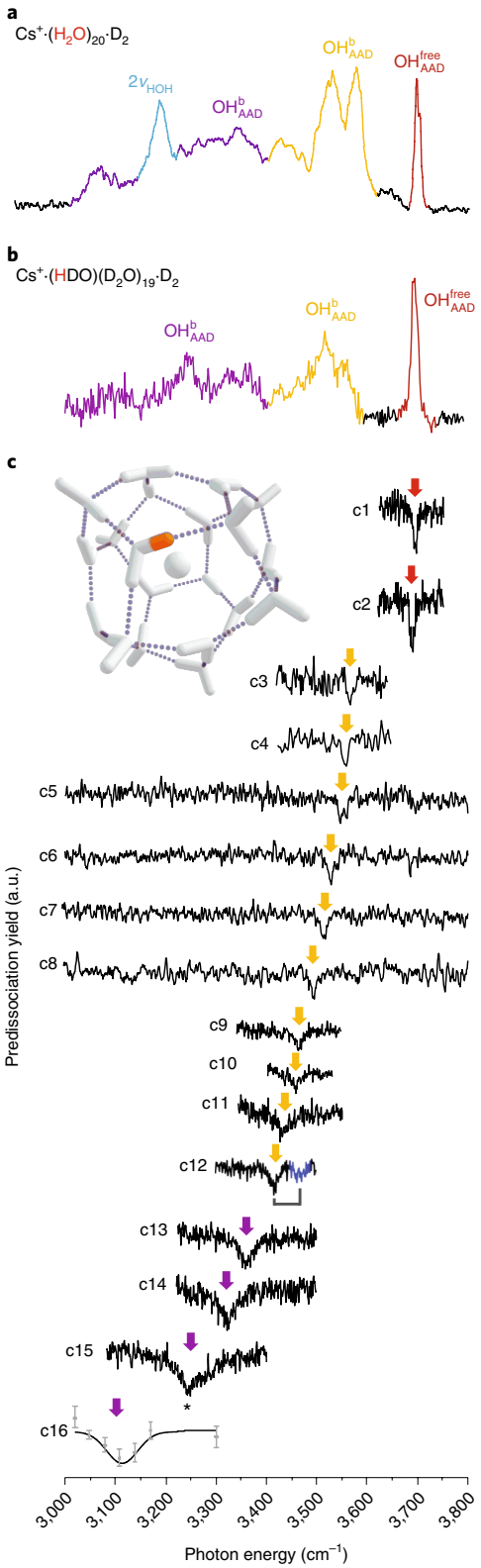

Fig. 2 | Isolating the spectral signatures of individual OH groups in the Cs^+·(HDO)$(D_2O)_{19}$ spectrum with IR-IR hole burning. a–c, The vibrational predissociation spectra of Cs^+·$(H_2O)_{20}$·D_2 (**a**) and Cs^+·(HDO)$(D_2O)_{19}$·D_2 (**b**), and the isotopomer-specific spectra of Cs^+·(HDO)$(D_2O)_{19}$·D_2 (**c**). The purple, turquoise and red colours highlight represent the bound OH (OH^b_{AAD}), HOH bend overtone ($2\nu_{HOH}$) and the free OH (OH^{free}_{AAD}) on the AAD water molecules, respectively, while the yellow bands are due to the bound OH stretches (OH^b_{ADD}) on the ADD water molecules. Isotopomer selective spectra c1–c16 of Cs^+·(HDO)$(D_2O)_{19}$ were obtained by probing at various locations indicated by the colour-coded arrows. The structure shows one example of the single OH group that is in a configuration that contributes to one of the yellow OH^b_{ADD} features. The depletion at the probed wavelength by the pump laser is typically ~50%, but falls to ~20% in the lowest energy bands. Trace c12 is expanded in Supplementary Fig. 4 to show more detail. The experimental frequencies are collected in Supplementary Tables 1 and 2. The asterisk in c15 denotes a sharper feature that is embedded in the broader lineshape. Probe positions and widths are reported in Supplementary Table 1. Trace c16 was taken with extensive averaging at representative points due to the low signal intensity in this energy range. The error bars indicate the range enclosed by ±1 s.d. a.u. (arbitrary units).

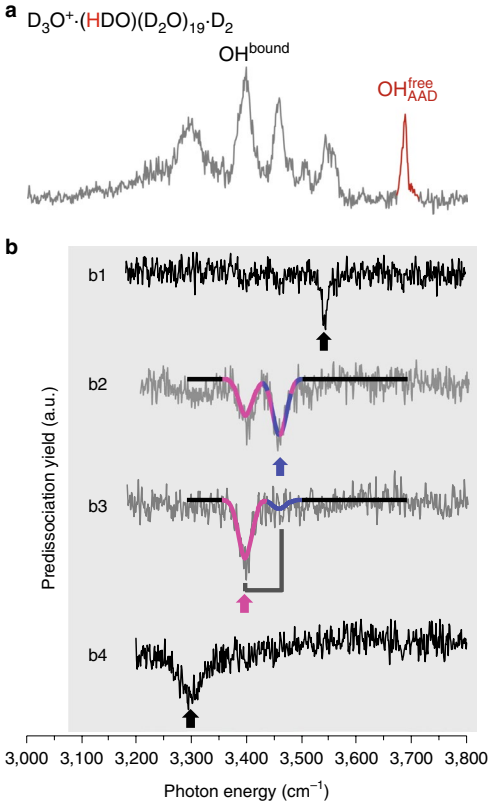

Fig. 3 | Isolating the spectral signatures of individual OH groups in the $D_3O^+\cdot(HDO)(D_2O)_{19}\cdot D_2$ spectrum, highlighting the appearance of a second feature in the isotopomer-specific spectra near 3,400 cm^{-1}. **a**, Non-selective spectra. **b**, The isotopomer-selective photobleach scans b1–b4 were obtained with the probe laser positions labelled by the arrows. The combination bands are labelled by brackets displaced from the OH stretching fundamentals on the lower energy side (b3). The simulated traces (coloured in b2 and b3) are overlaid on top of experimental data (grey traces), with a detailed explanation of the photoexcitation scheme given in Supplementary Fig. 4. Details about the simulation are included in Supplementary Section III. Probe positions and widths are reported in Supplementary Table 3.

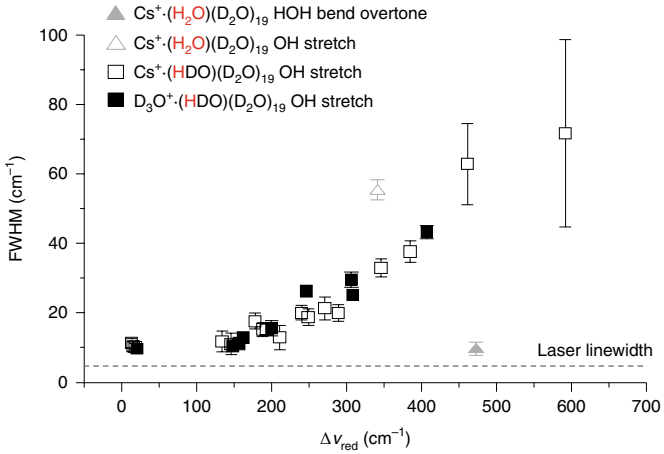

Fig. 4 | Dependence of experimental linewidths of OH stretching features on redshift. Values are derived from the dip features in Fig. 2c and Supplementary Fig. 5. The redshift of the OH frequency is relative to the gas-phase uncoupled free OH stretching fundamental at 3,607 cm^{-1}. The error bars are drawn at ±1 s.d. from the datapoints and correspond to the confidence interval associated with the Gaussian fits used to obtain the spectral width (Supplementary Fig. 5). The open triangle refers to the bound OH group and the filled triangle to the 0→2 overtone of the intramolecular HOH bend in $Cs^+\cdot(H_2O)(D_2O)_{19}\cdot D_2$. All the data are collected in Supplementary Tables 1 and 3.

it is clear that both systems display a very similar, approximately linear systematic increase in the bandwidths for redshifts ($\Delta\nu_{red}$) above ~150 cm^{-1}. The similarity in the behaviour of the two cage systems is interesting given that the nature of the charge accommodation (surface versus internal) is quite different in each case. Nonetheless, both cages are calculated at the harmonic level to display similar overall spectral profiles (Figs. 4 and 5 in Fournier et al.[40]) with the water molecules in the cage carrying a very small percentage of the charge (<0.02 and 0.005 electrons/water molecule for the H_3O^+ and Cs^+ cages, respectively)[42].

Note that asymptotic behaviour at low $\Delta\nu_{red}$ is limited by the bandwidth of the infrared laser (FWHM, ~5 cm^{-1}). The lineshapes in $D_3O^+\cdot(HDO)(D_2O)_{19}\cdot D_2$ are particularly well defined, as highlighted in Supplementary Fig. 5, and are well described with a Gaussian intensity distribution far outside the instrument resolution. Unfortunately, the signal-to-noise ratio does not allow a differentiation between Gaussian and Lorentzian lineshapes. It is important that at the experimental temperature (20 K), the thermal fluctuation is expected to be strongly suppressed, so that the lineshapes in the cold isotopomers are dominated by the relaxation dynamics at play in the vibrationally excited states. This can be seen in the temperature-dependent spectra of $D_3O^+\cdot(HDO)(D_2O)_{19}\cdot D_2$, in which the peak widths remain constant below 60 K (Supplementary Fig. 7). As such, this measurement provides a determination of the intrinsic character of the vibrational excitations with minimal contributions from thermal fluctuations, and therefore sets an upper limit on the coherence lifetimes (τ_v) of the OH stretching excitations at a low temperature, as well as the inherent complexities that arise from the excitation of combination bands. The approximate linear increase in width with redshift indicates that $\tau_v \propto \frac{1}{\Delta\nu_{red}}$, which approaches about 75 fs for the lowest frequency bands at around 3,100 cm^{-1}. This experimental approach cannot, however, establish the relative contributions of population relaxation (T_1) and pure dephasing (T_2^*) to these lifetimes.

Capturing the spectral behaviour of a local OH oscillator in a well-defined network environment has the significant advantage that we can address the detailed mechanics that underlie the relaxation dynamics. Moreover, that most of the lineshapes are relatively smooth indicates that the background states that contribute to the mixing are sufficiently dense to yield an effective continuum. This, in turn, suggests that the broadening can be addressed within the intramolecular vibrational relaxation mechanism in which the oscillator strength of a 'bright' OH stretching fundamental (at zero order) is diluted into a bath of dark states. As the bands increasingly broaden towards lower energies, at which the density of states is lower, we conclude that the main factor driving the increased widths derives from the matrix elements coupling the OH($v=1$) states to the bath. We note that the broadening is, indeed, a property of the OH stretching degree of freedom, as evidenced by the fact that the linewidth of the HOH bend overtone (FWHM ~10 cm^{-1}, filled triangle in Fig. 4) displayed by a single H_2O molecule in one of the $Cs^+\cdot(H_2O)(D_2O)_{19}$ isotopomers is much narrower than that of its bound OH group (FWHM ~56 cm^{-1}, open triangle in Fig. 4). Interestingly, the broadening of the bound OH stretch in H_2O falls well above the trend line for the isolated OH groups (open squares in Fig. 4), consistent with the expected acceleration in the relaxation rate due to mixing with the nearby overtone of the bend[29].

The systematic increase in the intrinsic linewidths with redshift raises the question as to whether these processes (shift and

broadening) are intimately connected. At an intuitive level, it seems plausible that the more redshifted OH oscillators are more strongly perturbed by the surrounding medium, and that this stronger coupling somehow leads to shorter lifetimes of the vibrationally excited states. This general theme was explored by Tainter et al.[19] in the context of the neutral water hexamer. They calculated how the frequencies of OH oscillators in each site are broadened by mechanical deformations in the network that are available to the cage isomer at low temperature (40 K). As such, we conclude the shifts largely reflect the local electric field along its OH bond axis, as it was determined that these structural displacements yield much larger fluctuations in the local electric fields when the net field is large. This leads to a situation in which the linewidths, indeed, increase monotonically with the redshift. This model predicts a non-linear dependence on redshift, but with an initial rate that is substantially larger than that observed here for the larger water cages, as illustrated by the comparison in Supplementary Fig. 8. Interestingly, the values for the neutral hexamer are closest to those found in the PD cages for the lowest frequency oscillators. Although it is beyond the scope of this experimental report to attempt a similar theoretical simulation of the anharmonic coupling, we note that the mechanical displacements of the 20 K water cages that give rise to such fluctuations in the electric fields are likely to involve vibrational zero-point motion[41,43]. In that case, the broadening is an unavoidable nuclear quantum effect that is intrinsic to the system, a phenomenon that has been well documented in a number of hydrogen-bonded cluster systems at low temperature[43,44].

In summary, we experimentally determined the spectral signatures of isolated OH groups embedded in an extended water network at low temperature. These transitions explore the full frequency range displayed by condensed phase and interfacial water. Double-resonance methods revealed the intrinsic lineshapes associated with each site, which appear as single features at the extremes of the diffuse OH envelope, but display a doublet structure near the centre of it, which are assigned to combination bands derived from excitation of soft modes of the cage. The fundamentals generally appear as bell-shaped distributions with widths that monotonically increase with the redshift in the centroid of the peak. These results establish upper bounds on the lifetimes of the OH($v=1$) states prepared by impulsive (coherent) excitation, which are on the order of 75 fs for the most redshifted bands around 3,100 cm^{-1}. This general trend can be rationalized by considering the strength of the local electric field at each site and the variation in this field caused by distortions of the cage, which points the way for more advanced theoretical treatments of these processes.

Methods

Materials and methods are detailed in the Supplementary Information.

Data availability

The authors declare that all data supporting the findings of this study are available within the paper and its Supplementary information files.

Online content

Any Nature Research reporting summaries, source data, extended data, supplementary information, acknowledgements, peer review information; details of author contributions and competing interests; and statements of data and code availability are available at https://doi.org/10.1038/s41557-019-0376-9.

Received: 27 July 2019; Accepted: 11 October 2019;
Published online: 25 November 2019

References

1. Paesani, F., Xantheas, S. S. & Voth, G. A. Infrared spectroscopy and hydrogen-bond dynamics of liquid water from centroid molecular dynamics with an ab initio-based force field. *J. Phys. Chem. B* **113**, 13118–13130 (2009).
2. Reddy, S. K., Moberg, D. R., Straight, S. C. & Paesani, F. Temperature-dependent vibrational spectra and structure of liquid water from classical and quantum simulations with the MB-pol potential energy function. *J. Chem. Phys.* **147**, 244504 (2017).
3. Auer, B. M. & Skinner, J. L. IR and Raman spectra of liquid water: theory and interpretation. *J. Chem. Phys.* **128**, 224511 (2008).
4. Skinner, J. L., Pieniazek, P. A. & Gruenbaum, S. M. Vibrational spectroscopy of water at interfaces. *Acc. Chem. Res.* **45**, 93–100 (2012).
5. Ni, Y. C., Gruenbaum, S. M. & Skinner, J. L. Slow hydrogen-bond switching dynamics at the water surface revealed by theoretical two-dimensional sum-frequency spectroscopy. *Proc. Natl Acad. Sci. USA* **110**, 1992–1998 (2013).
6. Nicodemus, R. A., Corcelli, S. A., Skinner, J. L. & Tokmakoff, A. Collective hydrogen bond reorganization in water studied with temperature-dependent ultrafast infrared spectroscopy. *J. Phys. Chem. B* **115**, 5604–5616 (2011).
7. Laage, D., Stirnemann, G., Sterpone, F. & Hynes, J. T. Water jump reorientation: from theoretical prediction to experimental observation. *Acc. Chem. Res.* **45**, 53–62 (2012).
8. Ashihara, S., Huse, N., Espagne, A., Nibbering, E. T. J. & Elsaesser, T. Ultrafast structural dynamics of water induced by dissipation of vibrational energy. *J. Phys. Chem. A* **111**, 743–746 (2007).
9. Steinel, T. et al. Water dynamics: dependence on local structure probed with vibrational echo correlation spectroscopy. *Chem. Phys. Lett.* **386**, 295–300 (2004).
10. De Marco, L., Fournier, J. A., Thamer, M., Carpenter, W. & Tokmakoff, A. Anharmonic exciton dynamics and energy dissipation in liquid water from two-dimensional infrared spectroscopy. *J. Chem. Phys.* **145**, 094501 (2016).
11. De Marco, L., Ramasesha, K. & Tokmakoff, A. Experimental evidence of Fermi resonances in isotopically dilute water from ultrafast broadband IR spectroscopy. *J. Phys. Chem. B* **117**, 15319–15327 (2013).
12. Asbury, J. B. et al. Dynamics of water probed with vibrational echo correlation spectroscopy. *J. Chem. Phys.* **121**, 12431–12446 (2004).
13. Stiopkin, I. V. et al. Hydrogen bonding at the water surface revealed by isotopic dilution spectroscopy. *Nature* **474**, 192–195 (2011).
14. Schaefer, J., Backus, E. H. G., Nagata, Y. & Bonn, M. Both inter- and intramolecular coupling of O–H groups determine the vibrational response of the water/air interface. *J. Phys. Chem. Lett.* **7**, 4591–4595 (2016).
15. van der Post, S. T. et al. Strong frequency dependence of vibrational relaxation in bulk and surface water reveals sub-picosecond structural heterogeneity. *Nat. Commun.* **6**, 8384 (2015).
16. van der Post, S. T. & Bakker, H. J. Femtosecond mid-infrared study of the reorientation of weakly hydrogen-bonded water molecules. *J. Phys. Chem. B* **118**, 8179–8189 (2014).
17. Bakker, H. J. & Skinner, J. L. Vibrational spectroscopy as a probe of structure and dynamics in liquid water. *Chem. Rev.* **110**, 1498–1517 (2010).
18. Skinner, J. L., Auer, B. M. & Lin, Y. S. Vibrational line shapes, spectral diffusion, and hydrogen bonding in liquid water. *Adv. Chem. Phys.* **142**, 59–103 (2009).
19. Tainter, C. J., Ni, Y., Shi, L. & Skinner, J. L. Hydrogen bonding and OH-stretch spectroscopy in water: hexamer (cage), liquid surface, liquid, and ice. *J. Phys. Chem. Lett.* **4**, 12–17 (2013).
20. Mallik, B. S., Semparithi, A. & Chandra, A. Vibrational spectral diffusion and hydrogen bond dynamics in heavy water from first principles. *J. Phys. Chem. A* **112**, 5104–5112 (2008).
21. Stenger, J., Madsen, D., Hamm, P., Nibbering, E. T. J. & Elsaesser, T. Ultrafast vibrational dephasing of liquid water. *Phys. Rev. Lett.* **87**, 027401 (2001).
22. Asbury, J. B. et al. Ultrafast heterodyne detected infrared multidimensional vibrational stimulated echo studies of hydrogen bond dynamics. *Chem. Phys. Lett.* **374**, 362–371 (2003).
23. Yang, N., Duong, C. H., Kelleher, P. J., Johnson, M. A. & McCoy, A. B. Isolation of site-specific anharmonicities of individual water molecules in the $I^-(H_2O)_2$ complex using tag-free, isotopomer selective IR-IR double resonance. *Chem. Phys. Lett.* **690**, 159–171 (2017).
24. Horvath, S. et al. Anharmonicities and isotopic effects in the vibrational spectra of X^-H_2O, ·HDO, and $·D_2O$ [X = Cl, Br, and I] binary complexes. *J. Phys. Chem. A* **114**, 1556–1568 (2010).
25. Duong, C. H. et al. Disentangling the complex vibrational spectrum of the protonated water trimer, $H^+(H_2O)_3$, with two-color IR–IR photodissociation of the bare ion and anharmonic VSCF/VCI theory. *J. Phys. Chem. Lett.* **8**, 3782–3789 (2017).
26. Lawrence, C. P. & Skinner, J. L. Vibrational spectroscopy of HOD in liquid D_2O. VII. Temperature and frequency dependence of the OH stretch lifetime. *J. Chem. Phys.* **119**, 3840–3848 (2003).
27. Gale, G. M., Gallot, G. & Lascoux, N. Frequency-dependent vibrational population relaxation time of the OH stretching mode in liquid water. *Chem. Phys. Lett.* **311**, 123–125 (1999).
28. Moilanen, D. E. et al. Water inertial reorientation: hydrogen bond strength and the angular potential. *Proc. Natl Acad. Sci. USA* **105**, 5295–5300 (2008).
29. Imoto, S., Xantheas, S. S. & Saito, S. Ultrafast dynamics of liquid water: energy relaxation and transfer processes of the OH stretch and the HOH bend. *J. Phys. Chem. B* **119**, 11068–11078 (2015).

30. Schulz, F. & Hartke, B. Dodecahedral clathrate structures and magic numbers in alkali cation microhydration clusters. *Chem. Phys. Chem.* **3**, 98–106 (2002).
31. Xantheas, S. S. Low-lying energy isomers and global minima of aqueous nanoclusters: structures and spectroscopic features of the pentagonal dodecahedron $(H_2O)_{20}$ and $H_3O^+(H_2O)_{20}$. *Can. J. Chem. Eng.* **90**, 843–851 (2012).
32. Buch, V. et al. The single-crystal, basal face of ice I_h investigated with sum frequency generation. *J. Chem. Phys.* **127**, 214502 (2007).
33. Smit, W. J. et al. Excess hydrogen bond at the ice–vapor interface around 200 K. *Phys. Rev. Lett.* **119**, 133003 (2017).
34. Yang, N., Duong, C. H., Kelleher, P. J., McCoy, A. B. & Johnson, M. A. Deconstructing water's diffuse OH stretching vibrational spectrum with cold clusters. *Science* **364**, 275–278 (2019).
35. Bailey, C. G., Kim, J., Dessent, C. E. H. & Johnson, M. A. Vibrational predissociation spectra of $I^-\cdot(H_2O)$: isotopic labels and weakly bound complexes with Ar and N_2. *Chem. Phys. Lett.* **269**, 122–127 (1997).
36. Leavitt, C. M. et al. Characterizing the intramolecular H^- bond and secondary structure in methylated $GlyGlyH^+$ with H_2 predissociation spectroscopy. *J. Am. Soc. Mass Spectr.* **22**, 1941–1952 (2011).
37. Okumura, M., Yeh, L. I., Myers, J. D. & Lee, Y. T. Infrared-spectra of the solvated hydronium ion: vibrational predissociation spectroscopy of mass-selected $H_3O^+\cdot(H_2O)_n\cdot(H_2)_m$. *J. Phys. Chem.* **94**, 3416–3427 (1990).
38. Yang, N., Duong, C. H., Kelleher, P. J. & Johnson, M. A. Unmasking rare, large-amplitude motions in D_2-tagged $I^-\cdot(H_2O)_2$ isotopomers with two-color, infrared–infrared vibrational predissociation spectroscopy. *J. Phys. Chem. Lett.* **9**, 3744–3750 (2018).
39. Wolke, C. T. et al. Isotopomer-selective spectra of a single intact H_2O molecule in the $Cs^+(D_2O)_5H_2O$ isotopologue: going beyond pattern recognition to harvest the structural information encoded in vibrational spectra. *J. Chem. Phys.* **144**, 074305 (2016).
40. Fournier, J. A. et al. Site-specific vibrational spectral signatures of water molecules in the magic $H_3O^+(H_2O)_{20}$ and $Cs^+(H_2O)_{20}$ clusters. *Proc. Natl Acad. Sci. USA* **111**, 18132–18137 (2014).
41. Fournier, J. A. et al. Vibrational spectral signature of the proton defect in the three-dimensional $H^+(H_2O)_{21}$ cluster. *Science* **344**, 1009–1012 (2014).
42. Fournier, J. A. et al. Snapshots of proton accommodation at a microscopic water surface: understanding the vibrational spectral signatures of the charge defect in cryogenically cooled $H^+(H_2O)_{(n=2-28)}$ clusters. *J. Phys. Chem. A* **119**, 9425–9440 (2015).
43. Johnson, C. J. et al. Microhydration of contact ion pairs in $M^{2+}OH^-(H_2O)_{n=1-5}$ (M = Mg, Ca) clusters: spectral manifestations of a mobile proton defect in the first hydration shell. *J. Phys. Chem. A* **118**, 7590–7597 (2014).
44. Hamm, P. & Stock, G. Nonadiabatic vibrational dynamics in the $HCO_2^-\cdot H_2O$ complex. *J. Chem. Phys* **143**, 134308 (2015).

Acknowledgements

We acknowledge extensive discussions with A. B. McCoy on the possible origins of the broadening, as well as unpublished results shared by S. Xantheas on variations in the low-energy structures available to the $Cs^+\cdot(H_2O)_{20}$ clusters. This work was supported by the National Science Foundation grant CHE-1900119 and carried out with the instrument developed under AFOSR DURIP grant FA9550-17-1-0267. The part of the study on the $H_3O^+(H_2O)_{20}$ cluster was carried out under US Department of Energy, Office of Science, Basic Energy Sciences, CPIMS Program under grant award DE-FG02-06ER15800 as part of a larger effort designed to determine the barriers for proton translocation through the cage structure. C.H.D. thanks the National Science Foundation Graduate Research Fellowship for funding under grant DGE-1122492.

Author contributions

M.A.J. conceptualized and supervised the experiments, N.Y., C.H.D. and P.J.K. performed the experiments, N.Y. analysed the data, performed calculations and wrote the simulation codes. All the authors discussed the results and worked on the manuscript.

Competing interests

The authors declare no competing interests.

Additional information

Supplementary information is available for this paper at https://doi.org/10.1038/s41557-019-0376-9.

Correspondence and requests for materials should be addressed to M.A.J.